Journal of Materials Chemistry A

COMMUNICATION

View Article Online
View Journal | View Issue

Cite this: J. Mater. Chem. A, 2015, 3, 9092

Received 22nd October 2014
Accepted 2nd December 2014

DOI: 10.1039/c4ta05675b

www.rsc.org/MaterialsA

Inkjet printing of $CH_3NH_3PbI_3$ on a mesoscopic TiO_2 film for highly efficient perovskite solar cells†

Shao-Gang Li,[a] Ke-Jian Jiang,*[a] Mei-Ju Su,[ab] Xue-Ping Cui,[ab] Jin-Hua Huang,[a] Qian-Qian Zhang,[ab] Xue-Qin Zhou,*[b] Lian-Min Yang[a] and Yan-Lin Song*[a]

An inkjet printing technique is successfully used to deposit a perovskite $CH_3NH_3PbI_3$ layer on a mesoscopic TiO_2 film. With combined optimization of the table temperature and the ink composition, a flat and uniform perovskite layer is realized on the TiO_2 film, and the corresponding photovoltaic device exhibits a high efficiency of 12.3% with an average value of 11.2% under AM 1.5G conditions. The current work demonstrates that the inkjet printing method is environmentally benign and cost-effective with reduced waste of the toxic Pb-containing materials encountered inevitably in the existing techniques during the device preparation.

Introduction

During the past two decades, there have been extensive investigations for cost-effective thin film solar cells as alternative technologies to conventional inorganic counterparts. Among the innovative technologies, perovskite solar cells based on hybrid organometal trihalide perovskites, in the form of (MA)$[PbX_3]$ (MA = $CH_3NH_3^+$; X = Cl, Br, or I), are emerging as a strong competitor, and the power conversion efficiency (PCE) rapidly increased from 3.8% to more than 16% in the last five years.[1–13] Recently, a certified PCE of 17.9% was reported by the National Renewable Energy Laboratory (NREL).[14] In addition, a higher efficiency of 19.3% was also reported by Yang's group.[15] In this solar cell, high crystallinity perovskite layers can be formed by a simple spin-coating method, functioning as desirable light absorbers with a direct and tunable band-gap. As ideal photovoltaic materials, they possess both high hole and electron transport ability, small exciton binding energy (~20 meV), and long carrier diffusion lengths (100–1000 nm).[16,17] At present, most of the perovskite layers were deposited on planar or mesoscopic metal oxide substrates by the spin-coating technique with a one-step or two-step approach.[1–7,9–13] Alternatively, a vacuum deposition technique was also employed to generate a highly flat and uniform perovskite film, exhibiting a PCE of up to 15.4%.[8,18] In the perovskite solar cells, the photovoltaic performance is greatly dependent on the perovskite film morphology, which relies on the deposition method, annealing process and additives employed.[19–28] Despite enormous progress made in the device design and performance, exploring a suitable printing technique for the controllable and scalable production of the perovskite layers is highly expected when considering their practical applications. To this end, an ultrasonic spray-coating technique was employed for the fabrication of planar heterojunction perovskite solar cells, exhibiting a high power conversion efficiency (PCE) of 11% with an average PCE of 7.3%.[29] Recently, a two-step method including spin-coating and inkjet printing processes was used for fabricating the perovskite film, delivering an efficiency of 11.60%.[30]

Inkjet printing is a material-conserving deposition technique used for control deposition of different materials dispersed or dissolved in solution, enabling easy and fast deposition of functional materials on various substrates with large-area.[31] Inkjet printing has been a popular choice in the fabrication of various optoelectronic devices including light-emitting devices, solar cells and field-effect transistors.[32–34] In the previous report, polymer:fluorine bulk heterojunction organic photovoltaic devices were fabricated by the technique, and some critical parameters, including solvent formulation and inkjet table temperatures, were studied to achieve high-quality inject printed photoactive layers.[33]

In this work, a perovskite $CH_3NH_3PbI_3$ film was deposited as a light absorber on a mesoscopic TiO_2 film for perovskite solar cells by means of an inkjet printing technique. The printing ink contains perovskite precursor methylammonium iodide (MAI) and lead iodide (PbI_2) dissolved in γ-butyrolactone. We investigated the effect of the printing table temperature on the morphology and structure of the perovskite film and the device

[a]Key Laboratory of Green Printing, Institute of Chemistry, Chinese Academy of Sciences, Beijing, 100190, China. E-mail: kjjiang@iccas.ac.cn; ylsong@iccas.ac.cn
[b]Collaborative Innovation Center of Chemical Science and Engineering, Tianjin, 300072, China. E-mail: zhouxueqin@tju.edu.cn

† Electronic supplementary information (ESI) available. See DOI: 10.1039/c4ta05675b

performance. We further investigated the effect of methylammonium chloride (MACl) as an additive used in the ink on the film morphology and the device performance. With combined optimization of both the parameters, a flat and uniform perovskite layer on the mesoscopic TiO_2 film was realized. The film has strong light harvesting capacity, and the corresponding device exhibited a high power conversion efficiency of 12.3% with an average value of 11.2% under AM 1.5 illumination. Our results demonstrate that the inkjet printing technique is an effective fabrication tool for highly efficient perovskite solar cells. More importantly, the drop-on-demand inkjet technique is environmentally friendly for the deposition of the perovskite film. In contrast, a considerable amount of toxic Pb-containing materials is discarded in the fabrication processes of the existing spin-coating, spray coating, and vacuum deposition.

Results and discussion

In our experiments, all the samples were built on transparent fluorine-doped tin-oxide (FTO) coated glass substrates, where a TiO_2 blocking layer (80 nm thick) and a TiO_2 mesoscopic layer (400 nm thick) were used, respectively. The samples were arranged on the table 1 mm below the inkjet printhead, and printed using a piezoelectric driven flatbet inkjet printer, as reported previously.[35] The printing ink consisted of MAI, PbI_2, and MACl with a molar ratio of $1 - x : 1 : x$ ($x = 0$–0.9), dissolved in γ-butyrolactone with a concentration of 35 wt%. During the printing, the samples were *in situ* heated on the platen at a fixed temperature under ambient conditions. After the inkjet printing, the samples were transferred into a N_2-filled glove-box for post-annealing. Finally, 2,2′,7,7′-tetrakis-(*N*,*N*-di-*p*-methoxyphenylamine)-9,9′-spirobifluorene (spiro-OMeTAD) was deposited as a hole transport layer, followed by evaporation of a gold back electrode. Full experimental details on the device fabrication and characterization can be found in the ESI.†

In the printing, high boiling γ-butyrolactone (b.p. = 206 °C) was selected as a solvent in the ink, on one hand, due to its high solubility for the perovskite precursor, on the other hand, preventing nozzle clogging of the printhead due to the solvent evaporation during the printing. Unlike the conventional spin-coating, where most of the solvent in the deposited film can be rapidly removed by centrifugal force during spin-coating, the inkjet printing films, however, are usually in a fluid state, containing a large amount of solvent upon printing. Thus, it is essential to speed up solvent evaporation from the wet film. Otherwise, the crystallization of the perovskite would be slowed down, leading to a large thickness variation of the film.[7] Thus, *in situ* heat treatment was applied to accelerate solvent evaporation during the printing. The table temperature was adjusted from 25 °C to 60 °C with a short duration of 2 minutes. In addition, a 400 nm thick mesoscopic TiO_2 film was used as a substrate for the perovskite printing. In this case, the printed perovskite precursor was restrained within the porous TiO_2 film after the solvent evaporation and further converted into the crystalline perovskite with a confined nanomorphology after post-annealing.[7] It should be noted that after the printing and *in situ* heat treatment, the precursor on the films could not be fully converted into the crystalline perovskite. Thus, all the samples were subjected to further post-annealing for the crystallization. The process was carried out at 100 °C for 10 minutes in a N_2 atmosphere after the deposition.

The influence of the table temperature on the morphology and structure of the perovskite film was examined by scanning electron microscopy (SEM). The ink used here consists of the perovskite precursor PbI_2 and MAI (molar ratio of 1 : 1) dissolved in γ-butyrolactone with a concentration of 35 wt%. At room temperature (25 °C), the printed film surface was intricately covered with various shapes of perovskite crystallites with distinct edges and corners, as shown in Fig. 1. The morphology is obviously different from that of the spin coated film, where disc-like crystals were observed.[6,9] The result implies that the printed film is wet, and the precursor has more time to distribute and self-assemble at the low printing temperature, favoring the perovskite crystallization. At a temperature of 40 °C, the film morphology was changed clearly. A large amount of round and flattened crystal plates were spread uniformly on the surface, similar to that of the spin-coated film.[19] As the temperature increased to 50 °C, the crystal plates became larger. Meanwhile, a lot of small perovskite crystallites appeared, resulting in relatively high substrate coverage. On further increasing the temperature to 60 °C, the plate size further increased, followed by abundant pinholes on the surface, probably due to the high solvent evaporation ratio at this temperature. The pinholes can deteriorate the photovoltaic performance in the resultant devices.[19,20] The results suggested that the film morphology would strongly relate to the table temperatures, and a temperature of 50 °C would be optimal for the printing.

The photovoltaic performance was measured for the devices prepared at different table temperatures. As shown in Table 1, device 1 with the film deposited at room temperature (25 °C)

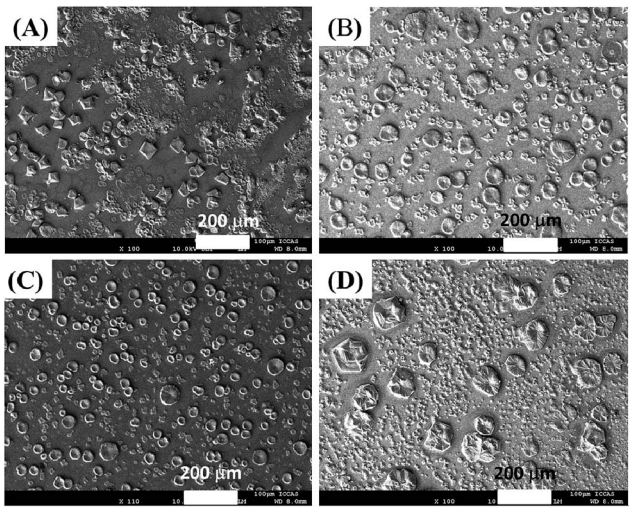

Fig. 1 Top-view SEM images of the inkjet printed perovskite (on mesoscopic TiO_2 films) deposited at 25 °C (a), 40° (b), 50 °C (c), and 60 °C (d).

Table 1 Photovoltaic performance of the devices prepared at different table temperatures and with various amounts of CH_3NH_3Cl in the printing solution

Device	Temperature/°C	X (CH_3NH_3Cl)	J_{sc}/mA cm^{-2}	V_{oc}/mV	FF	η/%
Device 1	25	0	13.21	820	0.61	6.6
Device 2	40	0	13.85	824	0.63	7.2
Device 3	50	0	14.71	826	0.65	7.9
Device 4	60	0	14.35	822	0.62	7.3
Device 5	50	0.3	15.73	844	0.64	8.5
Device 6	50	0.6	19.55	910	0.69	12.3
	50	0.6	18.91 ± 0.6	884 ± 40	0.67 ± 0.04	11.2 ± 0.7[a]
Device 7	50	0.9	18.85	868	0.66	10.8

[a] The average and the standard deviation for 20 samples.

gave a short-circuit photocurrent density (J_{sc}) of 13.21 mA cm^{-2}, an open-circuit voltage (V_{oc}) of 0.82 V, and a fill factor (FF) of 0.61 to yield a power conversion efficiency (PCE) of 6.6%, which is lower than those of the similar-structured devices prepared by the spin-coating method.[9] The low photovoltaic performance would come from the poor perovskite morphology with low substrate coverage. For device 2 with the film deposited at 40 °C, the conversion efficiency was considerably increased to 7.2%. At 50 °C deposition, device 3 gave a PCE of 7.9% with a J_{sc} of 14.71 mA cm^{-2}, a V_{oc} of 826 mV and a FF of 0.65, which is comparable to that of the device prepared by the spray-coating technique.[27] On further increasing the temperature to 60 °C for device 4, however, the performance slightly decreased to a PCE of 7.3%, probably due to the rough and pinhole-containing perovskite film leading to increased charge recombination in the device.

Recent reports demonstrated that the morphology of the perovskite film could be improved when halogen-containing additives were co-deposited with the perovskite precursors during the fabrication.[23–28] Here, varied amounts of the additive MACl were added to the precursor solution for further improving the morphology of the perovskite film. In the ink, PbI_2, MAI, and MACl were mixed with a molar ratio of $1 - x : 1 : x$ ($x = 0$–0.9), and the inkjet printing was carried out at a fixed table temperature of 50 °C. We observed that the colour of the film changed from light yellow to brown during the printing and the colour change became slow with the increase of the additive MACl in the ink previously.[24] After the printing, all the samples were post-annealed at 100 °C for 10 minutes and the morphology was investigated by SEM. As shown in Fig. 2, flower-like crystal plates with large size were observed upon addition of MACl at $x = 0.3$, as compared with the disc-like crystal plates with no MACl in the ink. The flower-like crystal plates possess a highly ordered internal structure, indicating a high crystallization of the perovskite when the additive was used. When x increased to 0.6, the crystals were flattened and interconnected to form a continuous uniform perovskite layer on the mesoporous TiO_2 surface with full surface coverage. The grain size in the perovskite upper layer was about 200–500 nm with a layer thickness of about 200 nm, as shown in Fig. 2f. On further increasing x to 0.9, the perovskite film seemed to undergo partial dewetting, resulting in relatively low surface coverage. The results indicate that the MACl additive can control the whole crystalline process and thus the morphology in the formation of the perovskite, and a suitable amount of the additive is critically important for the high-quality film with good surface coverage. For further investigating the nature of the perovskite film, X-ray diffraction (XRD) was conducted for the samples with the additive at $x = 0$ and 0.6. As shown in Fig. 3a, the XRD patterns are nearly the same for both the samples with main peaks located at 14.20, 20.08, 28.52, 31.96

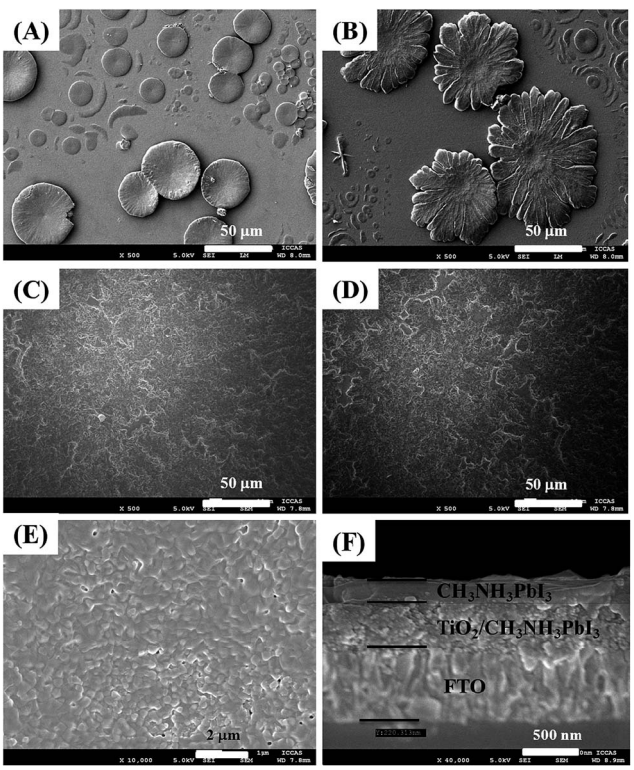

Fig. 2 Top-view SEM images of mesoporous TiO_2 films coated with the inkjet printed perovskite from the precursor solution with a molar ratio of $1 - x : 1 : x$ for PbI_2, MAI, and MACl, respectively, at $x = 0$ (a), $x = 0.3$ (b), $x = 0.6$ (c), $x = 0.9$ (d), and (e) $x = 0.6$, the scale bar is 1 μm, and the cross-sectional SEM image at $x = 0.6$ (f).

and 40.66°, assigned to the (110), (112), (220), (310), and (224) planes of the tetragonal perovskite $CH_3NH_3PbI_3$ structure, indicating that the addition of the additive would have no effect on the structure and composition of $CH_3NH_3PbI_3$. The diffraction peaks, however, became stronger in intensity upon the addition of the additive, as compared with those with no additive. This may be ascribed to the presence of the uniform perovskite upper layer with high crystallinity induced by the additive.[23] Fig. 3b shows the absorption spectra of the samples at $x = 0$ and 0.6. Clearly, the sample at $x = 0.6$ exhibits an enhanced absorbance in the long wavelength region (500–800 nm) because of the presence of the thick and high uniform upper layer as mentioned above, while the sample at $x = 0$ shows a relatively low absorbance in the region. The uniform upper layer on the mesoporous TiO_2 surface was desirable for improving the light harvesting capacity, and thus increasing the device photovoltaic perfomance[6,7] In the one-step spin-coating, the perovskite precursors were mainly limited in the porous TiO_2 films, and most of the superfluous solution on the surface was spun off during the deposition. Thus, it is almost impossible to control the morphology and structure of the resultant perovskite on the porous TiO_2 film, thus exhibiting poor substrate coverage. In the inkjet printing, a certain amount of the precursor solution can be well controlled as required, and completely used in the printing in principle. Thus, inkjet printing could well control the morphology and structure of the perovskite film.

To investigate the effect of the additive on the device performance, photovoltaic parameters were measured for the devices prepared with various amounts of the additive MACl in the printing solution, and the results are listed in Table 1. As can be seen from the data, the performance of device 5 ($x = 0.3$) was reasonably improved with a PCE of 8.5% in comparison with that (7.9%) of device 3 with no additive ($x = 0$). At $x = 0.6$ for device 6, all the photovoltaic parameters were augmented with a J_{sc} of 19.55 mA cm^{-2}, a V_{oc} of 910 mV, a FF of 0.69, and a PCE of 12.3%, which is the highest among the values for the mesoporous perovskite solar cells prepared by the standard

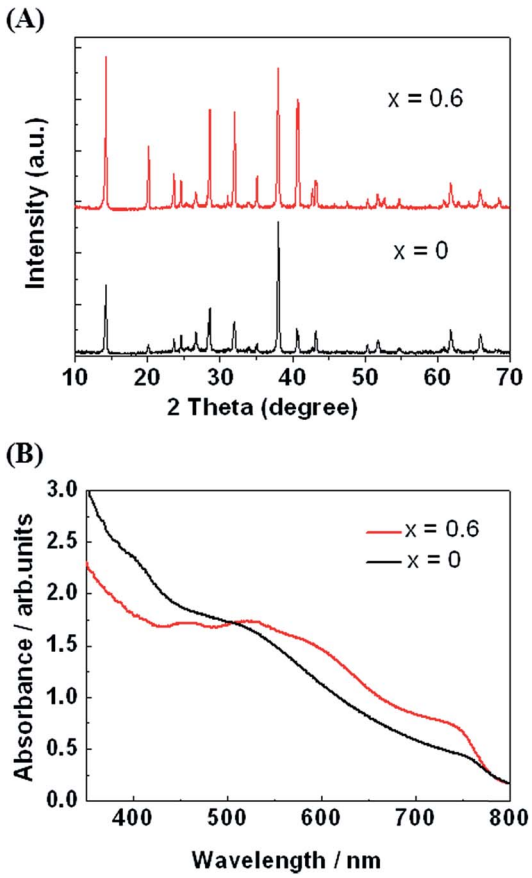

Fig. 3 XRD diffraction patterns (a) and UV-vis spectra (b) of the perovskite-coated TiO_2 films prepared at $x = 0$ and 0.6 from the precursor solution (the molar ratio of PbI_2, MAI, and MACl is $1 - x : 1 : x$).

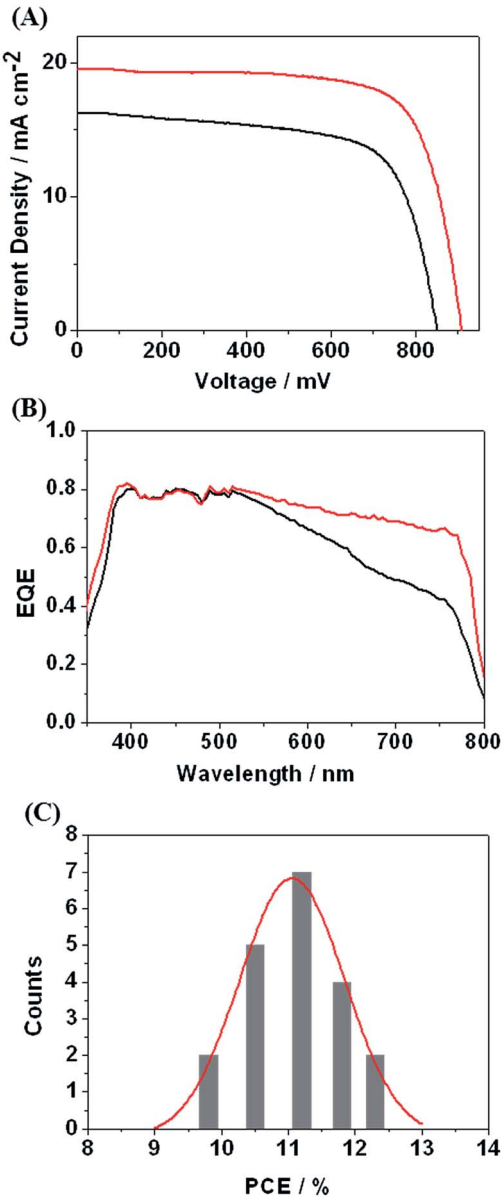

Fig. 4 I–V curves (a) and EQE spectra (b) of the devices prepared from the perovskite-coated TiO_2 films at $x = 0$ (black line) and 0.6 (red line), and histogram of PCEs for device 6 for 20 samples (c).

one-step spin-coating technology.[2–4] On further increasing the additives at $x = 0.9$ for device 7, however, the performance slightly decreased to 10.8%, probably due to the relatively low coverage as mentioned above. The current density–voltage (J–V) characteristics and the external quantum efficiency (EQE) spectra of device 3 and device 6 are shown in Fig. 4. The difference in the efficiency mainly came from the different J_{sc}s in the two devices, as shown in Table 1 and Fig. 4a. The external quantum efficiency (EQE) spectra show that both the devices present similar trends with the same amplitude at a short wavelength (300–500 nm), while at a long wavelength, device 6 exhibited significantly enhanced EQE. The difference in the EQE spectra can be explained by the different light harvesting capacity as shown in Fig. 3b, which is consistent with the difference in the J_{sc}s for both the devices. The results demonstrate that the uniform perovskite upper layer can effectively enhance light harvesting at long wavelength and improve the resultant photovoltaic performance because the perovskite materials exhibit weak absorption at long wavelength relative to the long wavelength.[6]

To check the device reproducibility, device 6 was prepared with 20 separate samples under the same conditions. As shown in Fig. 4c, the histogram of their PCEs presented high reproducibility with a low relative standard variation of 6.5% and a high average PCE of 11.2%. The high value of the average PCE and high reproducibility can be ascribed to the high-quality perovskite film prepared by the inkjet printing, demonstrating the great advantage of this fabrication method for the perovskite solar cells.

Conclusions

In the work reported here, an inkjet printing technique has been successfully used for the fabrication of a flat and uniform perovskite $CH_3NH_3PbI_3$ film on the mesoporous TiO_2 substrate. The role of the table temperature used in the printing was investigated, indicating that the *in situ* heating treatment is necessary in the printing. In addition, CH_3NH_3Cl as an additive in the printing solution was found to have a critical impact on the morphology and structure of the perovskite film formed. The film-optimized solar cell exhibited a best PCE of 12.3% under AM 1.5G conditions, with high reproducibility (a relative standard variation of 6.5%). The current work demonstrates that the inkjet printing can be an efficient and low cost approach for large-scale production of the perovskite solar cells. Meanwhile, the inkjet printing is an environmentally sound technique for the fabrication of perovskite solar cells. Further optimization, including device configuration and printing parameters, should improve the device performance, and the research is now in progress.

Experimental

Synthesis of CH_3NH_3I

10 ml of hydroiodic acid (55–58 wt%) was added dropwise to 24 ml of methylamine (33 wt%) and 100 ml of ethanol under a nitrogen atmosphere. A rotary evaporator was used to remove the solvent and crystallize methylammonium iodide (MAI). The precipitate was washed with diethyl ether three times. The resulting white powder was dried at 65 °C in a vacuum overnight.

Synthesis of CH_3NH_3Cl

19 ml of hydrochloride acid (33 wt%) was added dropwise to 24 ml of methylamine (33 wt%) and 100 ml of ethanol under a nitrogen atmosphere. A rotary evaporator was used to remove the solvent and crystallize methylammonium chloride (MACl). The precipitate was washed with diethyl ether three times. The resulting white powder was dried at 65 °C in a vacuum overnight.

Fabrication of perovskite-based solar cells

F-doped SnO_2 (FTO) coated glass was patterned by etching with zinc powder and 2 M hydrochloric acid. The substrates were carefully cleaned in ultrasonic baths of detergents, deionized water, acetone and ethanol successively. A compact TiO_2 blocking layer was deposited onto the surface of the cleaned FTO substrate by spin-coating of titanium diisopropoxide bis(acetylacetonate) solution (0.15 M, in 1-butanol) at 4000 r.p.m. for 30 s, dried at 125 °C for 5 min, then repeated twice with 0.3 M of titanium diisopropoxide bis(acetylacetonate) solution, followed by sintering on a hotplate at 500 °C for 30 min. After cooling to room temperature, the films were immersed in 0.02 M aqueous $TiCl_4$ at 70 °C for 30 min, followed by washing with ethanol and further sintering at 500 °C for 30 min. The mesoporous TiO_2 films were fabricated by spin-coating a 20 nm sized TiO_2 dispersion solution, which was prepared by diluting a commercial paste (18NR-T, Dyesol) by ethanol at 1 : 3.5 by weight. A 400 nm thick layer of TiO_2 was achieved *via* spin-coating at 3000 rpm for 30 s, followed by further sintering at 500 °C for 30 min. The perovskite films were inkjet printed by the perovskite precursor solution (35 wt% in γ-butyrolactone) with a molar ratio of $1 - x : 1 : x$ for PbI_2, MAI, and MACl, respectively. The inkjet printing was performed using a Dimatix Fujifilm DMP-2831 printer, including a piezoelectric-driven inkjet head with a motorized *xyz* stage. The printing frequency was set at 5.0 kHz and a customized waveform was used with a maximum voltage of 22 V and a pulse width of 8.5 μs. Mesoporous TiO_2 substrates were held on the platen at fixed temperatures ranging from 25 °C to 60 °C with 30–40% relative humidity (RH) in the printing chamber. After the deposition, the samples were transferred to a nitrogen-filled glovebox (<1 ppm O_2 and H_2O) for post-annealing. On the perovskite film, a layer of a hole transporting material was deposited by spin-coating (4000 rpm, 30 s) a spiro-MeOTAD (2,2′,7,7′-tetrakis(*N*,*N*-di-*p*-methoxyphenylamine)-9,9-spirobifluorene) solution in a N_2-filled glovebox. The spin-coating formulation was prepared as follows: to 1 ml of chlorobenzene were added 75 mg of spiro-MeOTAD, 30 μl of 4-*tert*-butylpyridine, and 20 μl of a stock solution of 500 mg ml^{-1} Li-TFSI in acetonitrile. Finally, an 80 nm thick Au was thermally evaporated as a back contact under a vacuum of 3×10^{-5} Torr. The device active area was 4 mm^2, determined by the overlap of the cathode and anode.

Characterization

XRD patterns were recorded by using an X-ray diffractometer (Rigaku, D/MAX RINT-2500) with a CuKα radiation source. The surface morphology of the films as well as cross-section was analyzed by using a JEM-7500F field-emission scanning electron microscope (SEM). Absorption spectra of the film samples were recorded by using a Shimadzu UV/vis 1800 spectrophotometer. Current–voltage characteristics were recorded by applying an external potential bias to the cell while recording the generated photocurrent with a Keithley model 2400 digital source meter. The light source was a 300 W collimated xenon lamp (Newport) calibrated with the light intensity to 100 mW·cm^{-2} under AM 1.5G solar light conditions by a certified silicon solar cell. The *J–V* curve was recorded by the reverse scans with a rate of 200 mV s^{-1}. The external quantum efficiency (EQE) for solar cells was performed using a commercial setup (PV-25 DYE, JASCO). A 300 W Xenon lamp was employed as a light source for the generation of a monochromatic beam. EQE spectra were recorded using monochromatic light without white light bias. Calibrations were performed with a standard silicon photodiode. EQE is defined by EQE(λ) = $hcJ_{sc}/e\varphi\lambda$, where h is Planck's constant, c is the speed of light in a vacuum, e is the electronic charge, λ is the wavelength in meters (m), J_{sc} is the short-circuit photocurrent density (A m^{-2}), and φ is the incident radiation flux (W m^{-2}).

Acknowledgements

The authors thank the National 863 Program (No. 2011AA050521), the continuous financial support of 973 Program (No. 2013CB933004, 2011CB932303 and 2011CB808400), the National Nature Science Foundation (Grant No. 21174149, 51373182, 51473173, 51173190, and 21121001), and the "Strategic Priority Research Program" of the Chinese Academy of Sciences (Grant No. XDA09020000).

Notes and references

1 A. Kojima, K. Teshima, Y. Shirai and T. Miyasaka, *J. Am. Chem. Soc.*, 2009, **131**, 6050.
2 M. M. Lee, J. Teushcer, T. Miyasaka, T. N. Murakami and H. J. Snaith, *Science*, 2012, **338**, 643.
3 H. S. Kim, C. R. Lee, J. H. Im, K. B. Lee, T. Moehl, A. Marchioro, S. J. Moon, R. Humphry-Baker, J. H. Yum, J. E. Moser, M. Grätzel and N. G. Park, *Sci. Rep.*, 2012, **2**, 591.
4 L. Etgar, P. Gao, Z. Xue, Q. Peng, A. K. Chandiran, B. Liu, M. K. Nazeeruddin and M. Grätzel, *J. Am. Chem. Soc.*, 2012, **134**, 17396.
5 J. H. Noh, S. H. Im, J. H. Heo, T. N. Mandal and S. I. Seok, *Nano Lett.*, 2013, **13**, 1764.
6 J. H. Heo, S. H. Im, J. H. Noh, T. N. Mandal, C. S. Lim, J. A. Chang, Y. H. Lee, H. J. Kim, A. Sarkar, M. K. Nazeeruddin, M. Grätzel and S. I. Seok, *Nat. Photonics*, 2013, **7**, 486.
7 J. Burschka, N. Pellet, S. J. Moon, R. Humphry-Baker, P. Gao, M. K. Nazeeruddin and M. Grätzel, *Nature*, 2013, **499**, 316.
8 M. Liu, M. B. Johnston and H. J. Snaith, *Nature*, 2013, **501**, 395.
9 J. H. Noh, S. H. Im, J. H. Heo, T. N. Mandal and S. I. Seok, *Nano Lett.*, 2013, **13**, 1764.
10 J. M. Ball, M. M. Lee, A. Hey and H. Snaith, *Energy Environ. Sci.*, 2013, **6**, 1739.
11 D. Liu and T. L. Kelly, *Nat. Photonics*, 2014, **8**, 133.
12 Q. Chen, H. Zhou, Z. Hong, S. Luo, H. S. Duan, H. H. Wang, Y. Liu, G. Li and Y. Yang, *J. Am. Chem. Soc.*, 2014, **136**, 622.
13 Z. Xiao, C. Bi, Y. Shao, Q. Dong, Q. Wang, Y. Yuan, C. Wang, Y. Gao and J. Huang, *Energy Environ. Sci.*, 2014, **7**, 2619.
14 NREL, (http://www.nrel.gov/ncpv/images/efficiency_chart.jpg), accessed on Oct. 15, 2014.
15 H. Zhou, Q. Chen, G. Li, S. Luo, T. Song, B. H. S. Duan, Z. Hong, J. You, Y. Liu and Y. Yang, *Science*, 2014, **345**, 542.
16 S. D. Stranks, G. E. Eperon, G. Grancini, C. Menelaou, M. J. P. Alcocer, T. Leijtens, L. M. Herz, A. Petrozza and H. J. Snaith, *Science*, 2013, **342**, 341.
17 G. Xing, N. Mathews, S. Sun, S. S. Lim, Y. M. Lam, M. Grätzel, S. Mhaisalkar and T. C. Sum, *Science*, 2013, **342**, 344.
18 C. W. Chen, H. W. Kang, S. Y. Hsiao, P. F. Yang, K. M. Chiang and H. W. Lin, *Adv. Mater.*, 2014, **26**, 6647–6652.
19 B. Conings, L. Baeten, C. D. Dobbelaere, J. Dhaen, J. Manca and H.-G. Boyen, *Adv. Mater.*, 2014, **26**, 2041.
20 A. Dualeh, N. Tétreault, T. Moehl, P. Gao, M. K. Nazeeruddin and M. Grätzel, *Adv. Funct. Mater.*, 2014, **24**, 3250.
21 P. Liang, C. Y. Liao, C. C. Chueh, F. Zuo, S. T. Williams, X. K. Xin, J. Lin and A. K. Y. Jen, *Adv. Mater.*, 2014, **26**, 3748.
22 N. J. Jeon, J. H. Noh, Y. C. Kim, W. S. Yang, S. Ryu and S. I. Seok, *Nat. Mater.*, 2014, **13**, 897.
23 Y. Zhao and K. Zhu, *J. Phys. Chem. C*, 2014, **118**, 9412.
24 P. W. Liang, C. Y. Liao, C. C. Chueh, F. Zuo, S. r T. Williams, X. K. Xin, J. Lin and A. K. Y. Jen, *Adv. Mater.*, 2014, **26**, 3748.
25 C. Zuo and L. Ding, *Nanoscale*, 2014, **6**, 9935.
26 H. Yu, F. Wang, F. Xie, We. Li, J. Chen and N. Zhao, *Adv. Funct. Mater.*, 2014, **24**, 7102–7108.
27 H. Zhou, Q. Chen, G. Li, S. Luo, T. B. Song, H. S. Duan, Z. Hong, J. You, Y. Liu and Y. Yang, *Science*, 2014, **345**, 542.
28 P. Docampo, F. Hanusch, S. D. Stanks, M. Döblinger, J. M. Feckl, M. Ehrensperger, N. K. Minar, M. B. Johnston, H. J. Snaith and T. Bein, *Adv. Energy Mater.*, DOI: 10.1002/aenm.201400355.
29 A. T. Barrows, A. J. Pearson, C. K. Kwak, A. D. F. Dunbar, A. R. Buckley and D. G. Lidzey, *Energy Environ. Sci.*, 2014, **7**, 2944.
30 Z. Wei, H. Chen, K. Yan and S. Yang, *Angew. Chem.*, 2014, **53**, 13239–13243.
31 M. Singh, H. M. Haverinen, P. Dhagat and G. E. Jabbour, *Adv. Mater.*, 2010, **22**, 673.
32 E. Tekin, H. Wijlaars, E. Holder, D. A. M. Egbe and U. S. Schubert, *J. Mater. Chem.*, 2006, **16**, 4294.
33 C. N. Hoth, S. A. Choulis, P. Schilinsky and C. J. Brabec, *Adv. Mater.*, 2007, **19**, 3937.
34 Y. Y. Noh, N. Zhao, M. Caironi and H. Sirringhaus, *Nat. Nanotechnol.*, 2007, **2**, 784.
35 Z. Zhang, X. Zhang, Z. Xin, M. Deng, Y. Wen and Y. Song, *Adv. Mater.*, 2013, **25**, 6714.